Characterisation of reactive magnesia and sodium carbonate-activated fly ash/slag paste blends

ash/slag paste blends

Ahmed F. Abdalqader, Fei Jin*, Abir Al-Tabbaa

Ahmed F. Abdalqader: PhD candidate, Department of Engineering, University of Cambridge,

Trumpington Road, Cambridge CB2 1PZ, United Kingdom

Fei Jin: Research Associate, Department of Engineering, University of Cambridge,

Trumpington Road, Cambridge CB2 1PZ, United Kingdom

Abir Al-Tabbaa: PhD, Professor in Department of Engineering, University of Cambridge,

Trumpington Road, Cambridge CB2 1PZ, United Kingdom

* Corresponding author

Email: leonking1987@gmail.com

Abstract: A system of alkali-activated fly ash (FA)/slag (AAFS) mixtures as a clinkerless cement was investigated with different dosages of Na_2CO_3, as a sustainable activator. The effect of incorporating various proportions of reactive magnesia (MgO) was also examined. Mechanical, mineralogical, and microstructural characterisation of the cement pastes was carried out using the unconfined compressive strength, X-ray diffraction, thermogravimetric analysis, infrared spectroscopy and scanning electron microscopy. It was found that the strength of Na_2CO_3 activated FA/slag mixtures generally increased with time and the Na_2CO_3 dosage. The hydration products were mainly C-(N)-A-S-H gel of low-crystallinity, which is rich in Al and may have included Na in its structure, and hydrotalcite-like phases. Adding reactive MgO in the mixes showed an accelerating effect on the hydration rate as suggested by the isothermal calorimetry data. Additionally, findings revealed variations on the strength of the pastes and the chemical compositions of the hydration products by introducing reactive MgO into the mixtures.

Keywords: Fly ash, Slag, Reactive magnesia, Sodium carbonate, Hydration, Microstructure

Highlights:

1. Na_2CO_3 activated fly ash/slag pastes were characterised by strength, hydration properties and microstructure.

2. Increasing the Na_2CO_3 content from 5% to 10% resulted in a remarkable increase in strength and hydration rate.

3. Incorporating reactive MgO to the blends has a notable influence on the reaction rate, the microstructure of the mixes and slight influence on the strength.

4. Hydration products include mainly C-(N)-A-S-H gel, hydrotalcite-like phases, calcite, and gaylussite.

1. Introduction

Portland cement (PC) and concrete are extensively used in the construction industry because of their remarkable technical performance and durability as well as their low cost. However, they are responsible for detrimental impacts on the environment because of their large consumption of natural resources, mass disposal of wastes, and the energy intensiveness and high carbon dioxide (CO_2) emissions of cement production. The production of PC, currently at more than 3 billion tonnes annually, is predicted to reach more than 4 billion tonnes per year by 2050 [1,2]. Approximately 0.85-1.0 tonne of CO_2 is emitted per tonne of cement clinker produced [3], which is responsible for 8-10% of the total man-made CO_2 emissions [4]. This places huge pressures on the cement and concrete industries to apply more sustainable practices. Optimising the production process of PC, using waste as fuel and raw materials, using renewable energy, and replacing the clinker partially or completely with industrial by-products, are all applied to minimise the negative environmental impact of PC production [5]. Another promising and more sustainable alternative is the use of alkali-activated cements (AACs) using industrial by-products. In this system, alkalis are introduced to silica aluminate materials (e.g., natural waste or industrial by-products) to raise the pH of the solution, thereby facilitating the breakage of the Si-O-Si and Al-O-Si bonds and starting the reactions to form a condensed structure [6,7]. Rashad [8] stated that AAC concrete compared to PC concrete could be 70% and 60% lower in global warming potential and energy consumption, respectively.

The extensively used materials for AACs are slag and fly ash (FA) [9]; the former is called alkali-activated slag (AAS) and the latter is known as geopolymer. Many previous studies investigated either alkali-activated slag or fly ash. As for the combined use of both, only a few studies were reported recently [10,11]. Given the limited global resources of the individual

3

by-products, combining them would provide a much bigger resource and counterbalance the disadvantages of each activation process [12]. The main hydration products of the alkali-activated FA/slag (AAFS) system are calcium silicate hydrates (C-S-H) gel, hydrotalcite-like phases, pirssonite ($Na_2Ca(CO_3).H_2O$), and calcite [12]. Chi and Huang [13] studied the binding mechanism and properties of AAFS mortars and concluded that better properties, compared to PC, have been obtained in terms of compressive strength, flexural strength and water absorption, although drying shrinkage was the major problem.

The most widely used activators are NaOH, waterglass (sodium silicate), and a combination of both. These activators, however, are a source of concerns because they are the most expensive component in the system and the primary source of greenhouse gas (GHG) emissions in the production of AAC concrete. In addition, these activators would cause the AACs to shrink and harden more rapidly than what is desirable [14]. The use of sodium carbonate (Na_2CO_3) as an activator is much less extensively studied in AACs although it has been shown that buildings made of Na_2CO_3-activated binders remained sound and increased in strength over their service life under conditions in which PC deteriorated rapidly [15]. Compared to other conventional activators, Na_2CO_3 yields a lower early age strength due to its lower pH but it can demonstrate higher strength at late ages than NaOH resulting from the effect of CO_3^{-2} ions [16], which lead to the formation of carbonated compounds that improve the mechanical strength [17]. Li and Sun [18] used Na_2CO_3 with or without NaOH to activate slag alone and a combination of slag and fly ash. The compressive strength of 10% Na_2CO_3-activated slag developed from 0 MPa at 3 days to 60 MPa at 28 days. Recently, Bernal *et al* [19] examined the activation mechanism of Na_2CO_3-activated slag. They proposed that the activation took place in three different stages starting with the dissolution of the slag and the formation of gaylussite and zeolite A in the first day. Then the reaction might go through an

94 extended induction period of 4-6 days with the conversion of gaylussite to $CaCO_3$ and the

95 formation of hydrotalcite. In the last stage, the precipitation of C-A-S-H gel started [19].

96 Magnesia, MgO, is mainly produced from the calcination of magnesite, $MgCO_3$, at different

97 temperatures resulting in different grades [20]. The use of hard burned MgO, calcined at 900-

98 1200°C, as a shrinkage compensating additive in the construction of the Baishan dam in

99 China in the mid of 1970s proved its efficiency and potential over the conventional

100 admixtures [21]. Ground granulated blastfurnace slag (GGBS) normally contains a high

101 content of MgO, which is in the slag glass network, sometimes up to 13%; whereas reactive

102 grade MgO (calcined under 1000 °C) or hard burned MgO (calcined at 1000–1400°C) are

103 often chosen for use as additives. Recent work found that reactive MgO can efficiently

104 activate the GGBS and showed higher strength than hydrated lime activated GGBS [22,23].

105 The main hydration products of MgO-GGBS system were C-S-H and hydrotalcite-like phases

106 [24]. The reaction of such system depends on the properties of MgO [24], which strongly

107 depend on the source of the precursor and the calcination history [25].

108 There are very limited reports regarding the effect of reactive MgO in AACs. Ben Haha *et al.*

109 [26] studied the effect of high inherent MgO content on alkali activated slag and found that

110 for waterglass activated slag paste, the compressive strength after 28 days increased by 50-

111 80% with increasing MgO content from 8 to 13%. This was because the higher MgO content

112 contributed to more hydrotalcite-like phases formed, resulting in up to 9% higher volume of

113 hydrates and a lower porosity. Additionally, Shen *et al.* [27] studied the properties of reactive

114 MgO modified alkali activated fly ash/slag cement (MAAFS) and concluded that the blends

115 can reach the strength standard of 42.5N. They also showed that adding MgO reduced the

116 shrinkage and cracking tendency due to its expansive hydration [27]. Kwok [28] studied the

117 effect of reactive MgO in Na_2CO_3-activated slag/limestone systems and found that replacing

118 limestone by reactive MgO remarkably increased the early strength and slightly increased the

119 28-day strength. The effect of MgO reactivity on the strength, shrinkage, and microstructure

120 of sodium silicate and sodium carbonate-activated slag was studied by [29–31]. They found

121 that adding reactive MgO into the AAC can effectively reduce the drying shrinkage and

122 increase the strength depending on the reactivity and the content of reactive MgO. However,

123 there is no literature on the role of reactive MgO in Na_2CO_3-activated slag/fly ash system.

124 Hence the aim of this paper is to examine the effect of combining reactive MgO and Na_2CO_3

125 for the activation of fly ash and slag blends on the strength, reaction kinetics, and hydration

126 products and microstructure.

2. Materials and Methods

128 The GGBS used was supplied by Hanson cement, UK, and has basicity ($K_b = \frac{CaO+MgO}{SiO_2+Al_2O_3}$) and

129 hydration modulus ($HM = \frac{CaO+MgO+Al_2O_3}{SiO_2}$) values of ~1.0 and ~1.60, respectively. The GGBS

130 was mainly amorphous with a broad hump in the 2θ region of $25-38°$ in the XRD pattern (not

131 shown). Merwinite ($Ca_3Mg(SiO_4)_2$) was identified as the only crystalline phase present. The

132 FA was obtained from Cemex, Rugby, UK and is classified to meet the requirements of the

133 British standard for use with PC (BS 3892: Part 1). The MgO was obtained from Richard

134 Baker Harrison, UK, and has a reactivity of 170 sec according to the acetic acid test, which

135 indicates medium reactivity according to the classification of Jin and Al-Tabbaa [25]. The

136 chemical compositions of all materials are shown in Table 1. Sodium carbonate was supplied

137 by Fisher scientific, UK as a powder and has the purity of 99%. It was dissolved in the mix

138 water until complete dissolution was reached.

139

Table 1 Chemical composition and physical characteristics of the materials used (based on the suppliers' datasheets)

Component	GGBS	FA	MgO
CaO %	39.24	6.8±3.6	1.9
SiO$_2$ %	36.79	49.3±6.2	0.9
Al$_2$O$_3$ %	11.51	24.1±0.4	0.1
Fe$_2$O$_3$	0.42	9.7±1.3	0.8
MgO %	8.10	1.1±0.2	93.5
SO$_3$ %	1.03	3.3±1.3	-
K$_2$O %	0.63	3.5±0.3	-
Na$_2$O %	0.37	1.2±0.1	-
SSA (m^2/kg)	545	2600	-

Clinkerless systems were prepared from GGBS, FA, and MgO and activated by Na$_2$CO$_3$. All mixes had a water to binder (w/b) ratio of 0.31. Each material is given an appropriate notation for simplicity. G, F, M, and N refer to GGBS, FA, MgO, and Na$_2$CO$_3$, respectively. The ratio of GGBS to FA was fixed at 3 parts to 1 part by weight. The proportion of MgO changed from 0 to 10% by replacing GGBS+FA and the content of Na$_2$CO$_3$ varied from 0-10% by the weight of the total binder as shown in Table 2.

Table 2 The mix proportions used in this study

Mix	GGBS %	FA %	MgO %	Na$_2$CO$_3$%
GFM5N0	71.25	23.75	5	0
GFM10N0	67.5	22.5	10	0
GFM0N5	75	25	0	5
GFM5N5	71.25	23.75	5	5
GFM10N5	67.5	22.5	10	5
GFM0N10	75	25	0	10
GFM5N10	71.25	23.75	5	10
GFM10N10	67.5	22.5	10	10

For the preparation of the paste samples, all the dry materials (GGBS, FA, and MgO) were mixed by hand in a bowl followed by 5 minutes' dry mixing in a mixer to which the Na$_2$CO$_3$ solution was then added. The mixer was stopped after 3 minutes of slow mixing, to collect

154 any unmixed solids scraped from the sides of the mixing bowl and the paddle into the bowl.

155 Then 2 more minutes of slow mixing and 5 minutes of fast mixing were applied to ensure

156 homogeneity. For each mix, the freshly mixed cement paste was placed into 40 x 40 x 40 mm

157 steel cubic moulds in three layers, and in between each layer the mixture was tapped with a

158 spatula for at least 25 times in two directions to remove the air voids. The samples were

159 demoulded after 2 days of curing and then cured in a water tank at temperatures between 20 ±

160 2 °C until the designed testing age. The demoulding time was done after 48 hrs because some

161 mixes were too soft to be demoulded after 24 hrs in agreement to [32].

162 Isothermal calorimetry experiments were conducted using a TAM Air Isothermal calorimeter,

163 at a base temperature of 20 ± 0.02 °C. Fresh paste was mixed externally, weighed into an

164 ampoule, and immediately placed in the calorimeter, and the heat flow was recorded for the

165 first 140 hrs of reaction. All values of heat release rate were normalised by total weight of the

166 paste.

167 The compressive strength testing was carried out using Controls Advantest 9 with a maximum

168 capacity of 250 kN and a loading rate of 2400 N/s. Triplicate cubes were tested at ages of 3, 7,

169 28, 56 and 90 days and the strength reported was an average of the three specimens.

170 Immediately after the compressive strength test at 28days, selected samples for

171 microstructural analyses were immersed in acetone for three days in order to stop any further

172 hydration. Then the samples were filtered to remove the acetone followed by vacuum drying

173 in a desiccator. The samples were then put in the oven at 60°C for at least 24 hrs. Thereafter,

174 part of the samples was crushed and ground in the agate mortar until passing the 75 μm sieve.

175 The powders obtained were sealed in plastic vials for further analysis.

176 Powder X-Ray diffraction (XRD) was employed to identify the crystalline phases in the

177 sample. The ground powders were placed on glass microscope slides onto which acetone was

178 dripped. After the acetone evaporated, the sample was affixed to the slide and placed in the

179 Siemens D500 X-ray diffractometer with a CuKα source operating at 40 kV and 40 mA,

180 emitting radiation at a wavelength of 1.5405 Å. The scanning regions were between 2θ values

181 of 5 to 60°, at a resolution of 0.02°/step. Thermogravimetric analysis (TGA) were conducted

182 using 20±2 mg powder under static air in an open alumina crucible heated at 10 °C/min over

183 the range of 40-1000°C on a Perkin Elmer STA6000 machine. Attenuated Total Reflectance

184 Fourier Transform Infrared (ATR-FTIR) spectra of the samples were taken using Perkin Elmer

185 FTIR Spectrometer Spectrum 100 Optica. Spectra were collected in transmittance mode from

186 4000 to 600 cm^{-1}at a resolution of 1cm^{-1}. Fractured surface specimens obtained from

187 mechanical testing were examined by scanning electron microscope (SEM) conducted on a

188 JEOL model JSM-820. Prior to SEM testing, the samples were mounted onto metal stubs

189 using carbon paste and coated with gold film to ensure good conductivity. The accelerated

190 voltage was set at 10 kV. Additionally, backscattered electron microscopy and energy

191 dispersive X-ray analysis (EDX) were carried out on the 28-day samples using FEI Nova

192 NanoSEM FEG at 15 kV accelerating voltage and a working distance of 5 mm. The samples

193 were impregnated in epoxy resin before polishing and coated with carbon.

3. Results and Discussions

194

3.1. *Unconfined Compressive Strength (UCS)*

195

196 The compressive strengths of all the mixes at ages of 3, 7, 28, 56, and 90 days are shown in

197 Fig. 1. The compressive strengths of samples containing no Na_2CO_3 were far lower than the

198 other mixes at all ages. However, it also demonstrates that even with the absence of the alkali

199 activator (black lines), MgO can activate the slag/FA blends effectively since the 3-day

200 strength of 10 % MgO activated slag/FA blends reached ~9 MPa. This is in agreement with

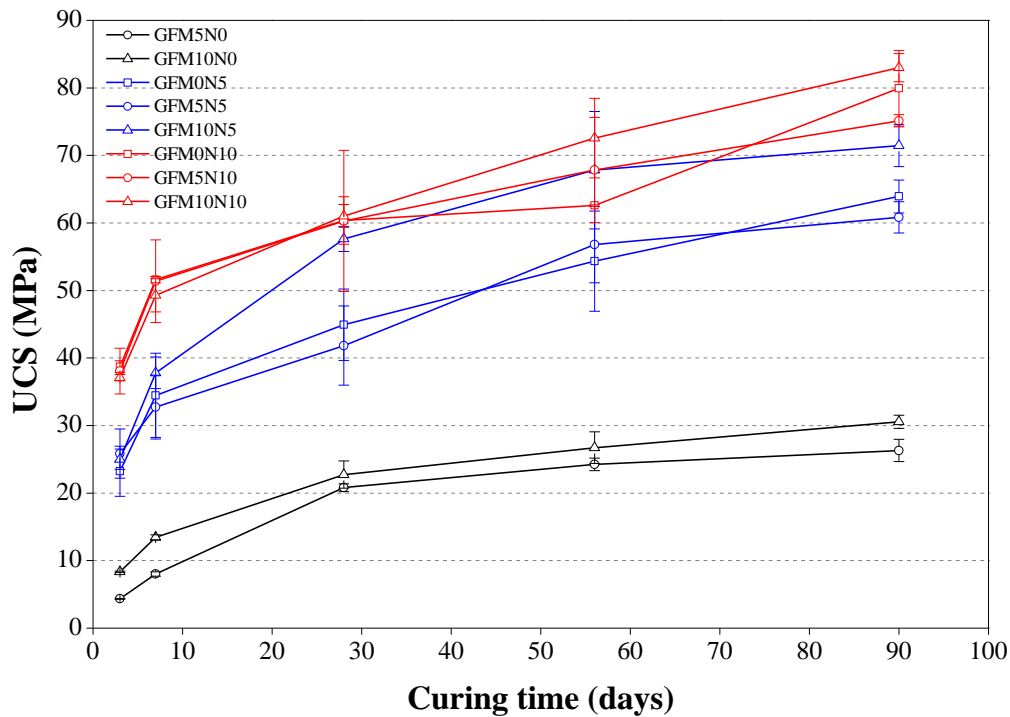201 the findings of [22,33,34].

Figure 1. UCS of AAFS cements at different ages

202 Fig.1 also presents the effect of MgO on the strengths of blends activated by 5% (blue lines)

203 and 10% (red lines) Na_2CO_3. Adding 5% of MgO (denoted with circles) had a marginal effect

204 on strength, while an increase of the MgO content to 10% (denoted with triangles) remarkably

205 increased the strength, especially after 28 days. The positive influence of MgO on the strength

206 could be attributed to its contribution in forming hydrotalcite which densifies the

207 microstructure [26,29]. Jin *et al.* [29] also showed the enhancement of strength by adding

208 reactive MgO into the Na_2CO_3 activated slag pastes. The addition of MgO to alkali activated

209 systems does not yield to strength loss as have been observed in PC-based systems [35,36].

210 This is because that MgO in alkali activate systems can react with the dissolved ions from the

211 aluminosilicate precursors to yield hydrotalcite-like phase or magnesium silicate hydrate gel

212   [24,29] while in PC systems it reacts separately with water to form brucite ($Mg(OH)_2$), which

213   is weaker than the strength-giving phase in PC [36].

214   It is also shown in Fig. 1 that adding Na_2CO_3 effectively activated the binders especially when

215   used at 10%. The range of the compressive strengths at early ages highly depended on the

216   Na_2CO_3 dosage. There is steep strength gain before 7 days followed by a relatively gradual

217   and almost linear gain up to 90 days for these mixes with Na_2CO_3, with final 90-day strength

218   of over 60-70% higher than the 7-day strength; whereas for mixes without Na_2CO_3, only a

219   slight strength gain was obtained after 28 days. The early age strength improvement by

220   Na_2CO_3 can be attributed to the higher pH of the pore solutions which accelerate the

221   dissolution of slag and FA. The remarkable strength development at later ages can be

222   attributed to the effect of carbonate ions as proposed by [15]. These data suggest that

223   activating slag/FA with Na_2CO_3 and incorporating MgO can yield strengths as high as 60

224   MPa at 28 days and as high as 80 MPa at 90days.

225   In the very few available reports about the strength of formulae activated by Na_2CO_3, lower

226   strength have been reported following similar conditions of the current study [19,28,32,37],

227   although they reported higher strength in special curing conditions[38]. Therefore, emphasis

228   in this work is placed on the fact that no high-temperature curing (all samples cured at room

229   temperature) or complicated fabrication techniques (autoclave curing, humidity chamber

230   curing, etc...) were used, making these formulae both practical for large-scale usage and of

231   reduced environmental impact. Therefore, the greatly reduced environmental impact, the

232   simplicity of manufacture, and the use of natural reactants (Na_2CO_3) are all reasons for further

233   investigation of these materials.

3.2. *Isothermal Calorimetry*

The heat release curves of mixes containing different percentages of MgO are shown in Fig. 2. There is an initial pre-induction period, associated with the partial dissolution of the slag and fly ash. This period is then followed by an extended induction period where little heat evolution was taking place. It is clear that increasing the activator dosage and the MgO content shortened this period. This indicates that the addition of MgO and increasing the activator dosage accelerate the reaction rate. The mix with 10% MgO led to higher heat of reaction (Fig. 2b) which means that an increased precipitation of reaction products occurred. The MgO content of slag has recently been identified to play a vital role in the kinetic of the reaction of alkali activated slag binders [39]. A high intensity heat evolution process between 40-70 h and 30-60 h in binders containing 5% Na_2CO_3 and 10% Na_2CO_3, respectively, was identified. This peak refers to the acceleration and deceleration processes when the precipitation of voluminous reaction products occurs, thereby releasing a significant heat of reaction. The occurrence and timing of this period explain the need for keeping the samples in the moulds up to 48 hours before demoulding and confirm that the formation of the strength-giving phases takes place during the first 48 hours. These results are different from [19], where the pre-induction and induction periods extended to more than 100 h, or sodium silicate-activated slag [26], which suggests that that the reaction kinetic is not only dependent on the alkaline activator but also on the chemical and physical properties of slag.

12
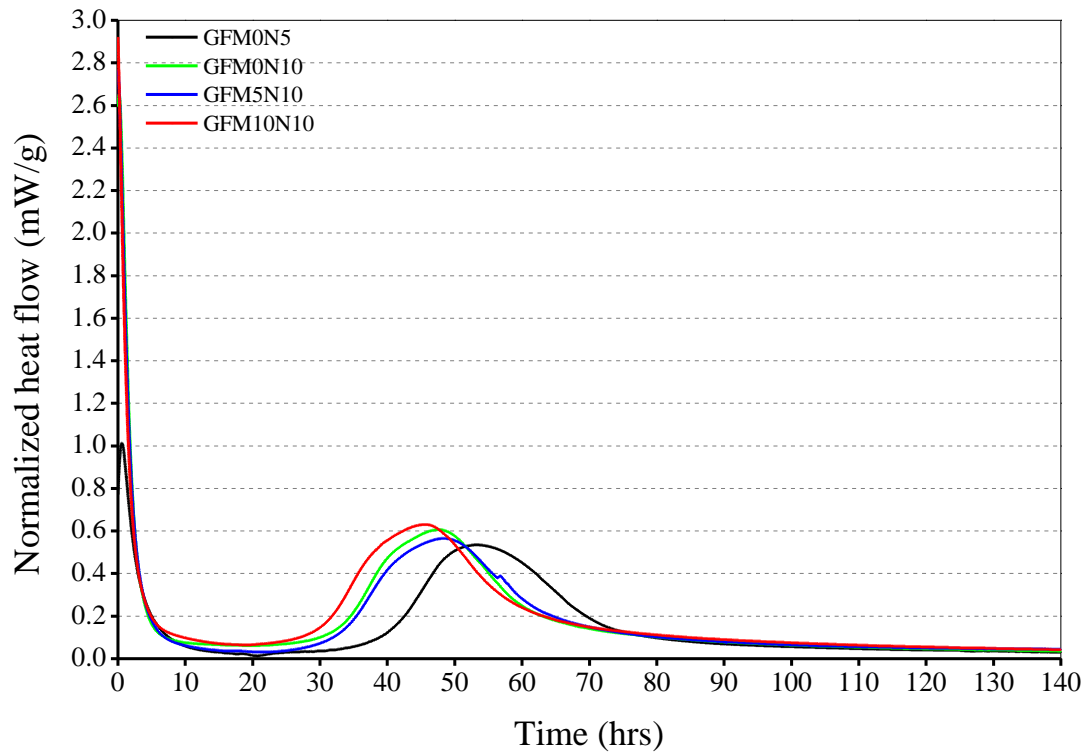
(a)
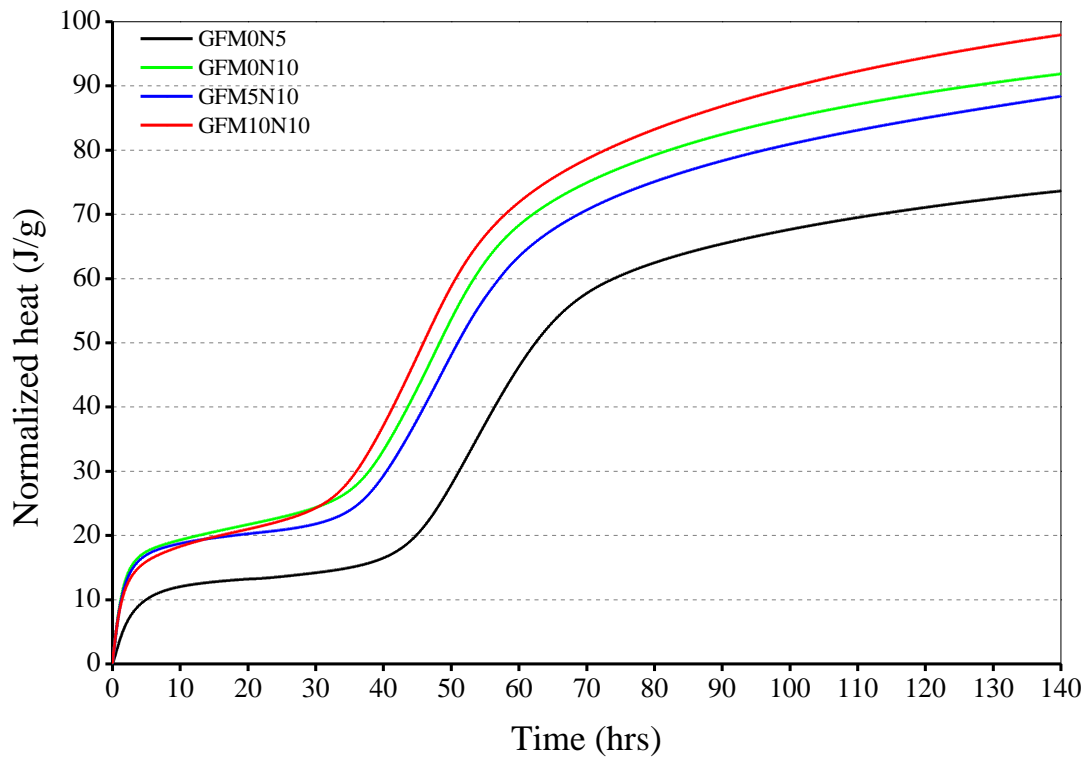
(b)

Figure 2. Heat release rate (a) and cumulative heat release (b) of different mixes

3.3. Hydration Products

The evolution of crystalline phases in the mixes at different ages is shown Fig. 3. In samples cured for 3 days (Fig. 3a), the broad hump present in the non-hydrated slag in the 2θ region of 25-38° slightly diminished during the first days of hydration and a new diffuse peak at about $2\theta = 29.5°$ appeared. This peak is assigned to C-S-H phase or calcite. C-S-H is generally considered to be poorly crystalline but its crystallinity in alkali-activated slag has already been reported by [40]. However, calcite occurrence is possible due to the recarbonation of Ca with CO_3^{2-} ions as reported by [15,37] along with other calcium carbonate polymorphs such as vaterite and aragonite[19]. Another main crystalline phase is the double salt gaylussite $(Na_2Ca(CO_3)_2.5H_2O)$, which is known to form as a natural evaporite in alkali lake waters [41]. The formation of such phases implies that at early ages there is a preferential reaction between the dissolved CO_3^{2-} and the Ca^{2+} released from the partial dissolution of the slag.

(a)

14
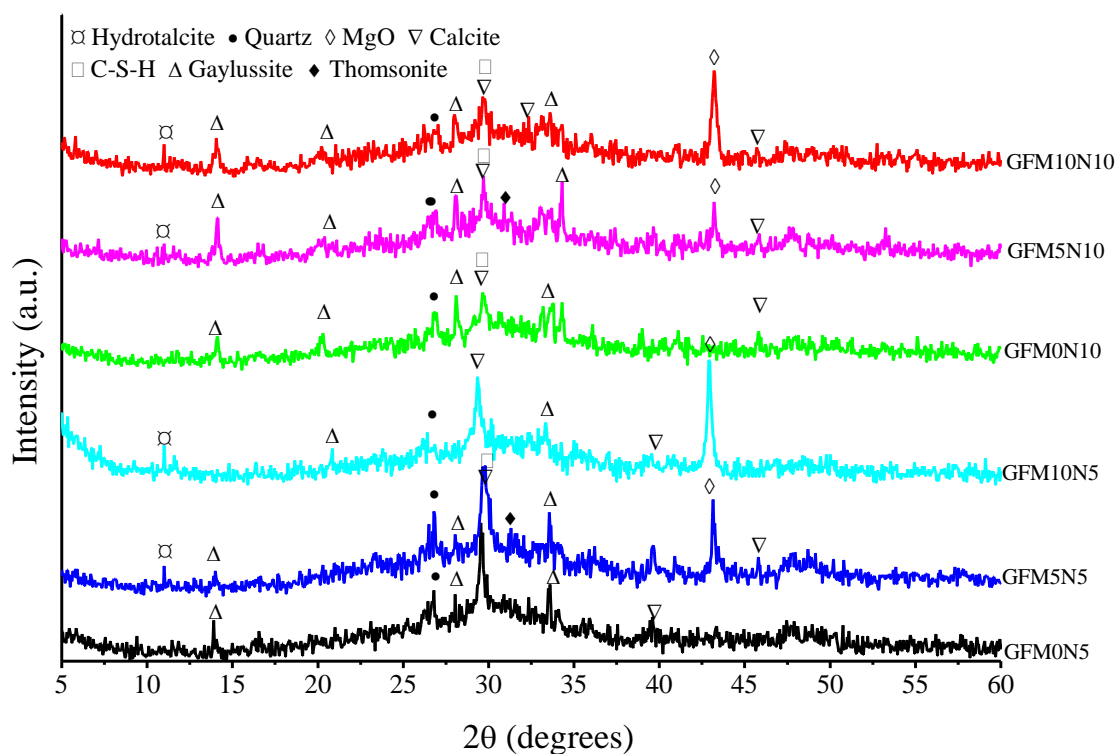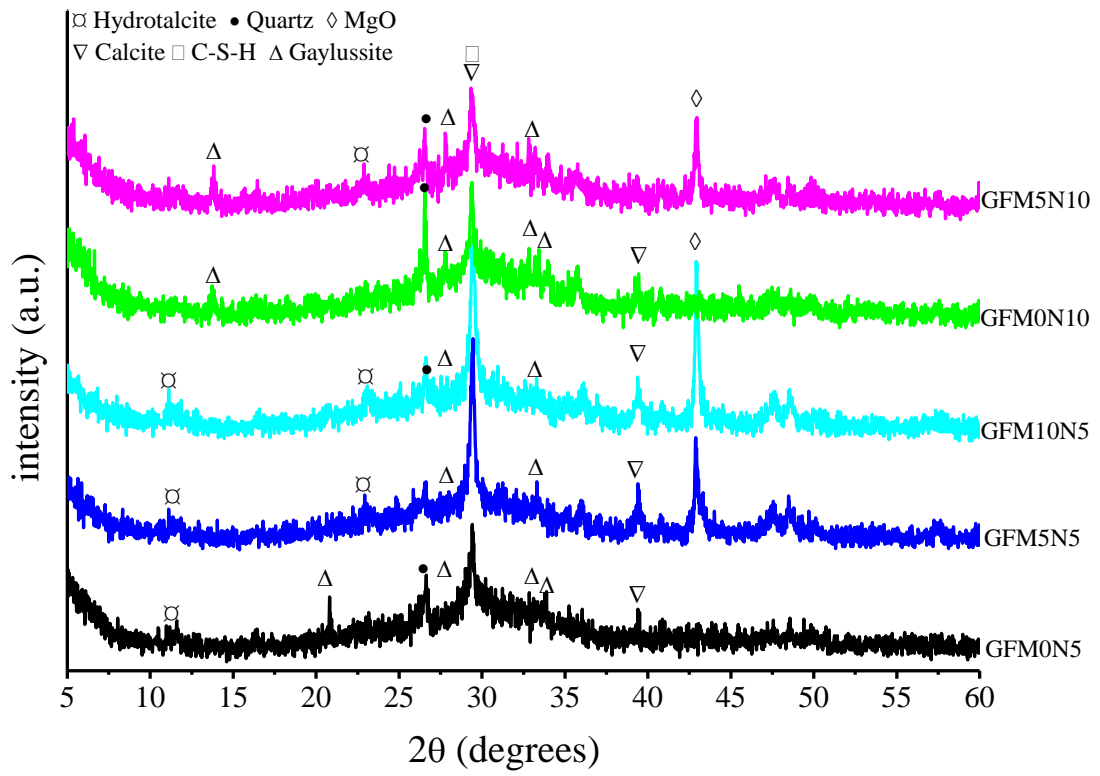
(b)
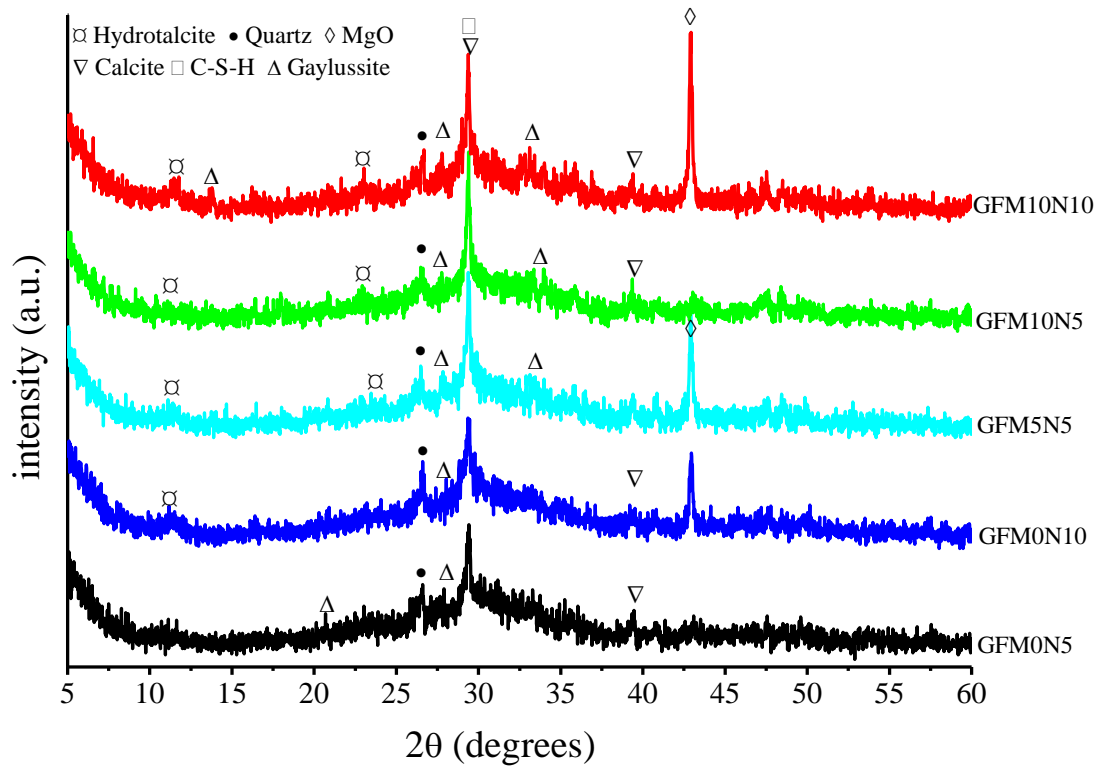
(c)

Figure 3. XRD of cement pastes at (a) 3 days, (b) 28 days, and (c) 180 days

15

265 Additionally supply from MgO could enhance the formation of hydrotalcite as it is defined as

266 an Mg-Al double-layered hydroxide. Also the presence of FA increased the uptake of Al to

267 form the hydrotalcite and C-(N)-A-S-H gel as some traces of thomsonite

268 ($NaCa_2Al_5Si_5O_{20} \cdot 6H_2O$) was observed and confirmed by TGA (see below). Thomsonite has

269 been identified in carbonated alkali-activated slag binders [42]. In addition, unreacted MgO

270 and some quartz, indicating the presence of unreacted FA, were also observed.

271 After 28 days of curing (Fig. 3b), the peaks of gaylussite disappeared on mixes containing

272 only 5% Na_2CO_3 and decreased on mixes containing 10% Na_2CO_3. Also the intensities of

273 calcium carbonate phases decreased possibly due to the formation of more C-A-S-H and

274 hydrotalcite like phases.

275 Significant increase in the intensities of the reflections assigned to hydrotalcite and C-A-S-H

276 along with the decrease of quartz and MgO were observed at 180 days (Fig 3c). It is clear that

277 the presence of MgO lead to the formation of more hydrotalcite-like phases and it seems that

278 after this extended curing age that the C-A-S-H gel and hydrotalcite-like phases were the

279 major hydration products, which agrees with the findings of [12,16,19,28,37]. Moreover,

280 there was no clear evidence of the presence of any magnesium carbonate in these blends as

281 reported by [27] or brucite reported by [26] which indicates that the presence of MgO in these

282 system only lead to the formation of hydrotalcite-like phases or M-(A)-S-H gels intermixed

283 with the main gel as will be discussed later. The activation of slag and FA initially consists of

284 breakdown of the covalent bonds Si-O-Si and Al-O-Si [43]. Dissolved Mg^{2+} ions then either

285 reacts with the broken bonds to form M-S-H or hydrotalcite like phases, thereby hindering the

286 precipitation of brucite [29]. This behaviour has been reported with adding reactive magnesia

287 to slag and silica fume [33,44,45].

288   The TG curves in Fig.4 show that four main humps were observed. It was found that the

289   weight loss increased with time for all samples. The first peak observed in the DTG curves

290   was at 85-105°C and is attributed to C-S-H dehydration [46]. This is consistent with the

291   removal of free evaporable water which is present in the pores of the geopolymer gel

292   products, either C-(A)-S-H type or N-A-S-H (zeolite-like) gels [47]. The main mass loss peak

293   between 300°C and 400°C is due to the decomposition of hydrotalcite [16]. The loss at 500-

294   600°C could be due to either the dehydration of thomsonite [48], M-S-H gel [29], or the

295   decomposition of poorly crystallised phase of calcite [37,49]. The temperature range of 600-

296   800 °C is the decomposition range of various carbonate-containing phases including

297   hydrotalcite, magnesium carbonate, and calcium carbonate [29]. These results are in good

298   agreement with the XRD results presented above. The increase of the hydrotalcite peak with

299   increasing the MgO content and with curing age was observed. The disappearance of the peak

300   at 500-600°C indicates that this phase was transformed with extended curing to other phases,

301   e.g., low crystalline calcite (vaterite) phases could be converted to a more stable phase such as

302   calcite [19].

303   The total weight loss (indicating the chemically bound water content) and the bound water

304   content in C-S-H are often used as a measurement of the hydration extent of blended cements

305   [50]. The calculated weight losses from TG data at different ages were summarised in Table

306   3, where the total weight loss was denoted as Δm. It can be seen that increasing the activator

307   dosage significantly increased the hydration degree at all ages. Increasing the content of MgO

308   increased slightly the hydration degree which could indicate that the presence of MgO

309   promoted the formation of more hydration products or products with more chemically bound

310   water. However, the contents of C-S-H and Δm of the mix made of GFM10N5 was lower

311   than those of GFM5N5 after 28 days of curing. This could be due to the reduced slag/FA

312 content replaced by MgO, leading to less C-S-H formed, although the strength of GFM10N5

313 was higher than that of GFM5N5. The improved strength could be attributed to the pore

314 filling effect of the unhydrated MgO, resulting in denser microstructure. Besides, the weight

315 loss associated to hydrotalcite-like phases increased with increasing MgO contents at 28 days.

316 The reduction of these values at 28 days compared to 3 days values could be due to the

317 overestimation of the weight loss associated to this peak as it overlapped with the third peak

318 as shown in Fig. 4a. It was found the total weight loss after 180 days did not change

319 significantly but the most apparent feature at this age was the disappearance of the third peak

320 as shown in Fig. 4c.
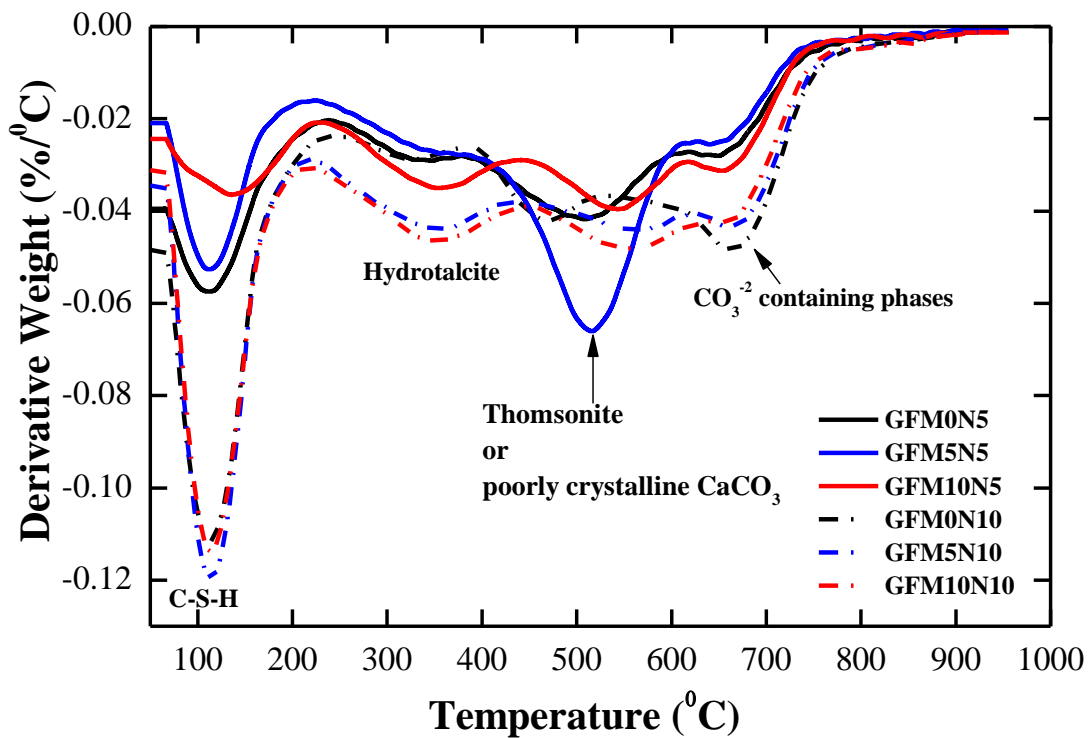
(a)
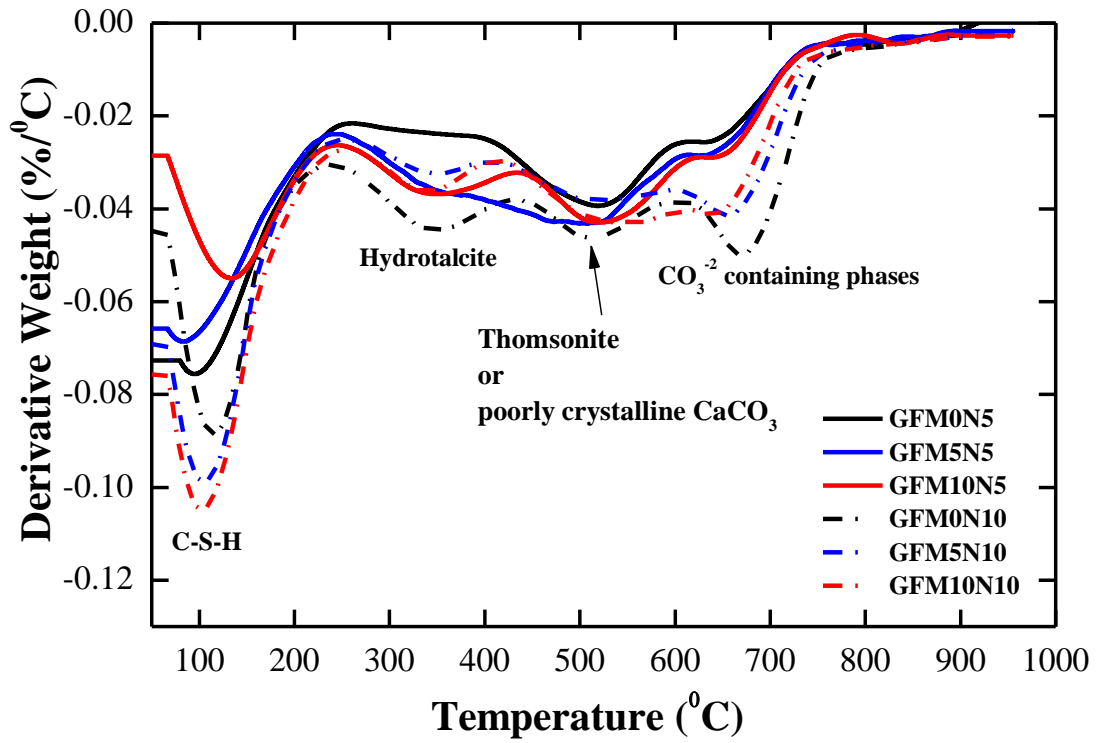
(b)
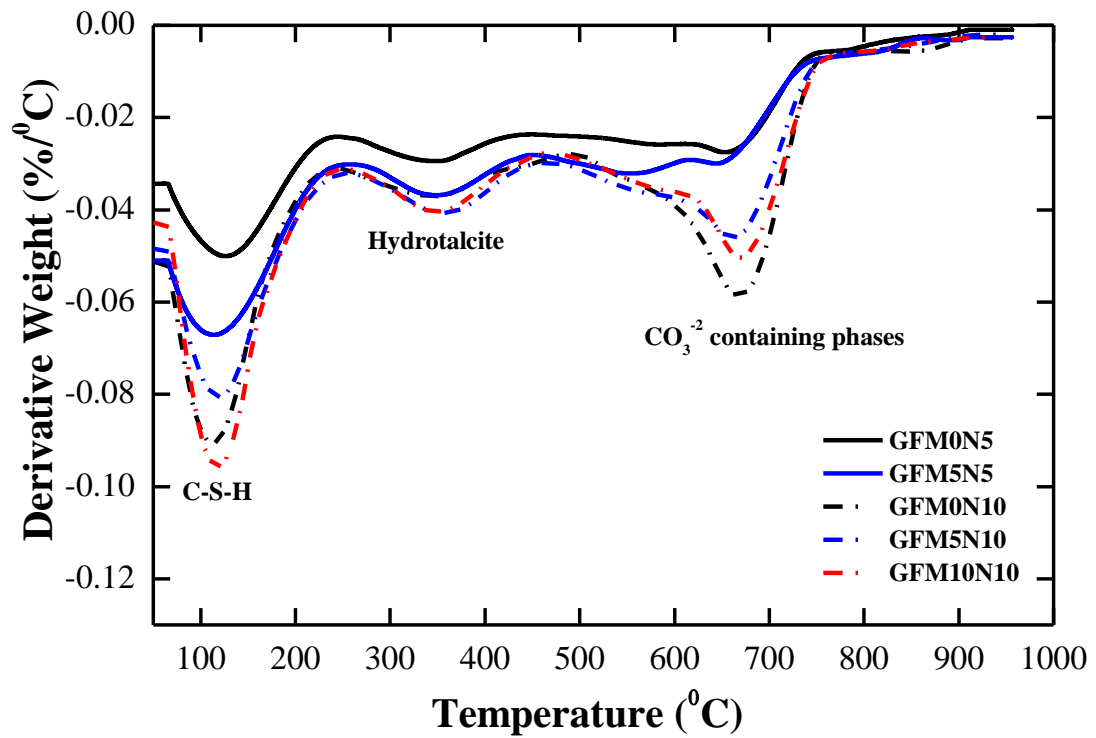
(c)

Figure 4. DTG of the mixes at (a) 3 days, (b) 28 days, and (c) 180 days

Table 3. Weight losses calculated from TGA

Blend	Weight loss					
	3 days			28 days		
	C-S-H	Ht	Δ m	C-S-H	Ht	Δ m
GFM0N5	4.5	3.05	12	5.8	2.38	12.75
GFM5N5	3	2.66	10.7	6.1	3.39	15
GFM10N5	3.1	3.13	10.3	4.75	3.46	13.75
GFM0N10	5	3.02	15.5	6.25	3.06	16.25
GFM5N10	5.5	4.16	15.9	7.9	3.12	16.75
GFM10N10	6	4.27	15.5	8	3.17	16.75

322

323 The FTIR spectra for the 28-day samples are presented in Fig.5. All the spectra show very

324 similar bands, suggesting a very similar nature of hydration products irrespective to the

325 activator dosage and MgO content used. The figure indicates major bands systems at

326 approximately 3400, 1650, 1450, 970, and 860 cm^{-1}. The structure of molecular water in the

327 alkali activated fly ash/slag system is characterized by the O-H stretching band, from 3,200 to

328 3,700 cm^{-1}, while the bending of the chemically bonded H-O-H is located at 1,650 cm^{-1} [47].

329 Noticeable bands at 1450 and 860 cm^{-1} suggest the presence of CO_3^{2-}, which can be attributed

330 to the presence of calcite or hydrotalcite as detected by both XRD and TGA. The strongest

331 band in the region of 1000-900 cm^{-1} corresponds to the asymmetric stretching vibration of Si-

332 O-T (T = tetrahedral Al, Si). The position of this band is consistent with both the C-(A)-S-H

333 structure formed by the activation of slag in alkaline media [11,51], and the N-A-S-H gels

334 formed in geopolymer systems derived from fly ash [52]. The typical band of these binding

335 gels in slag and FA is between 950 and 1100 cm^{-1} but the shift towards a lower wavenumber

336 indicates the reduced content of calcium in the gel formed from the activation of the slag and

337 increased incorporation of Al into this gel due to the dissolution of the FA [47]. Nevertheless,

338 the absence of the absorption band around 1000 to 1100 cm^{-1} indicates that the typical

339 structure of N-A-S-H gels is not formed within the hydration products.

The effect of MgO on the gel nanostructure as displayed by the FTIR spectra in Fig. 5 was more determinant in mixes activated by 5% Na_2CO_3. The principal band associated with Si-O-T near 970 cm^{-1} is broader in GFM10N5 than in GFM5N5 and GFM0N5. This confirms that this mix is more disordered than the others, which indicates the wide distribution of the SiQ^n (mAl) units occurring in these structures due to the incorporation of MgO. Besides, it is noted that this Si-O stretching band shifted progressively towards greater wavenumber from 950 cm^{-1} for GFM0N5 samples to 980 cm^{-1} and 985 cm^{-1} for GFM5N5 and GFM10N5, respectively. These values shift to higher wavenumber could be due to the decreasing of Al substitution in silicate network [53,54] which may be caused by the reaction of MgO and Al-O to form Ht.
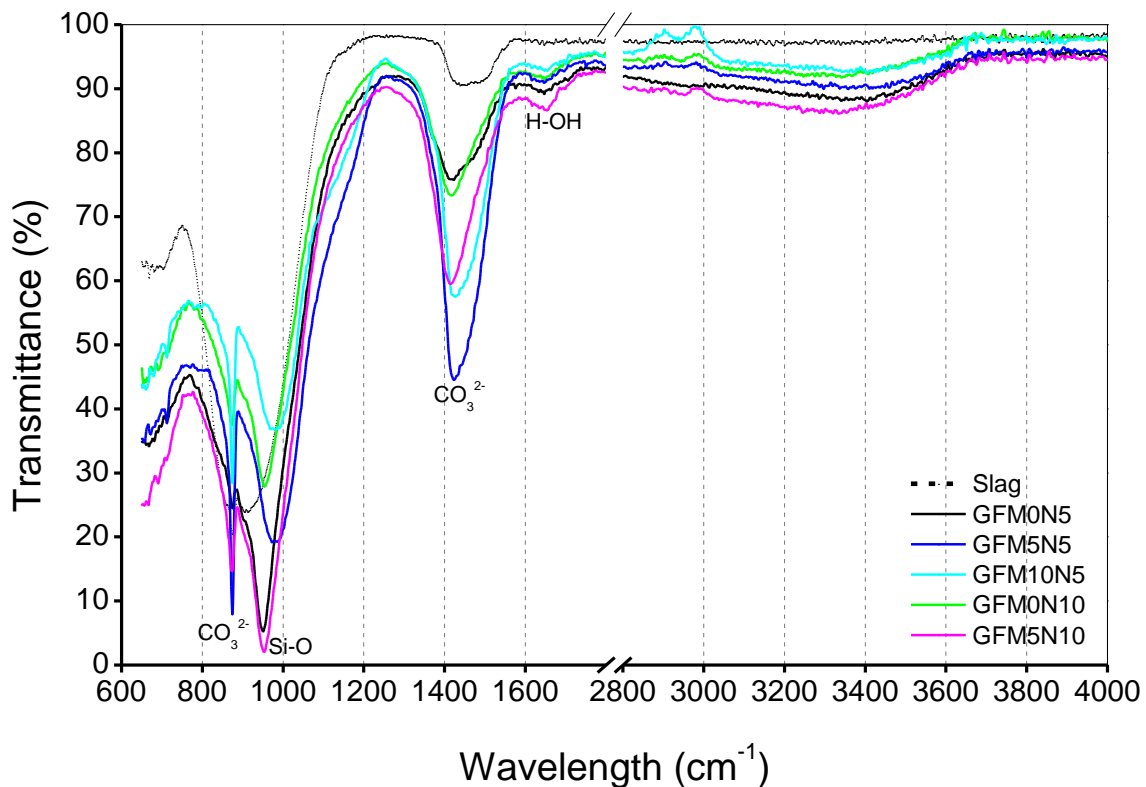
Figure 5. FTIR spectra of selective mixes 28 days

352 The FTIR bands of mix GFM0N10 at different ages is presented in Fig. 6. No clear changes

353 in the bands have been observed with the curing age. However, there was a slight shift of the

354 band at 950 cm^{-1} at 3 days to a higher wavenumber of 975 cm^{-1} at 28 days and 180 days

355 indicating more cross-linked and highly siliceous gels due to the reaction of fly ash
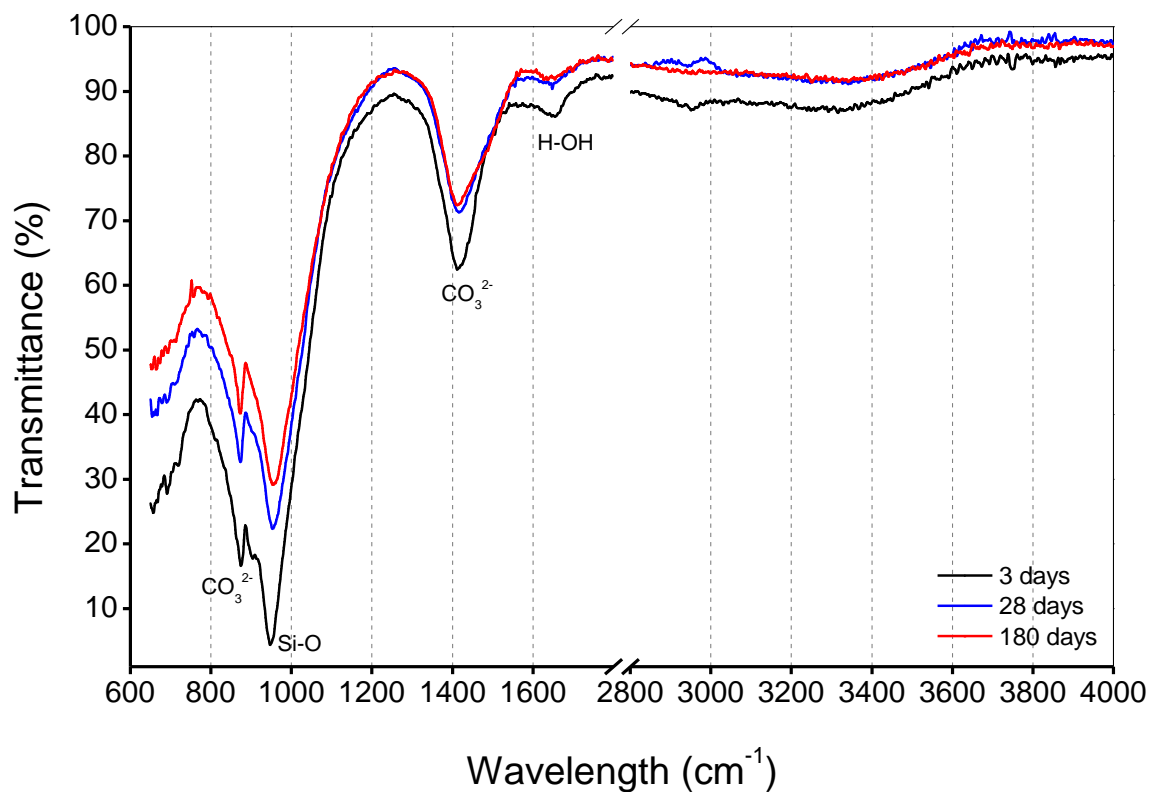
Figure 5. FTIR spectra of the GFM0N10 blend at different ages

356 **3.4.   *Microstructural Analysis***

357 The microstructures of the mixes were quite similar. The micrograph of blends without

358 Na$_2$CO$_3$ (Fig.7a) shows a loose network and many unhydrated slag grains, which explains the

359 low strength of such blends. Mixes containing both MgO and Na$_2$CO$_3$ had a denser

360 microstructure as shown in Fig.7b-d. Some unreacted fly ash particles were shown in the

361 matrixes.

22

(a)

(b)

(c)

(d)
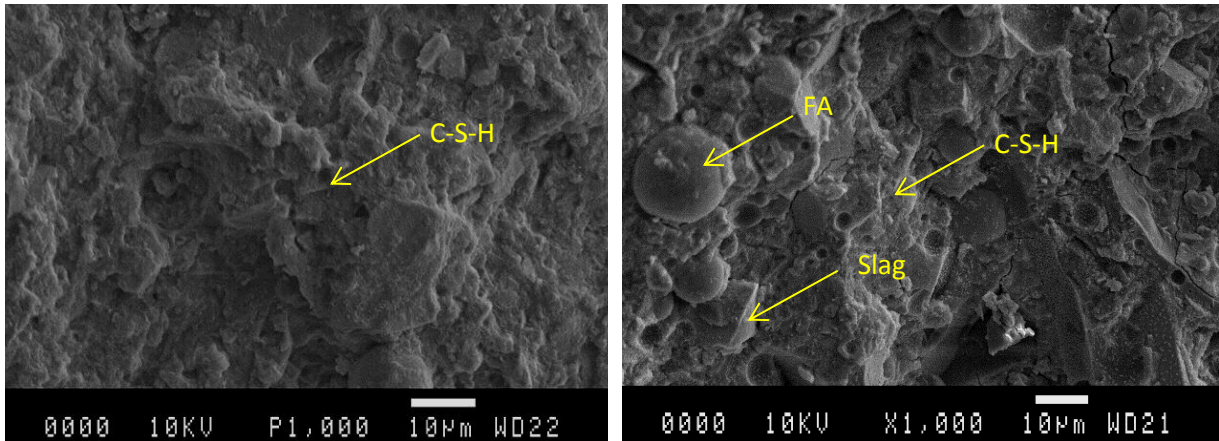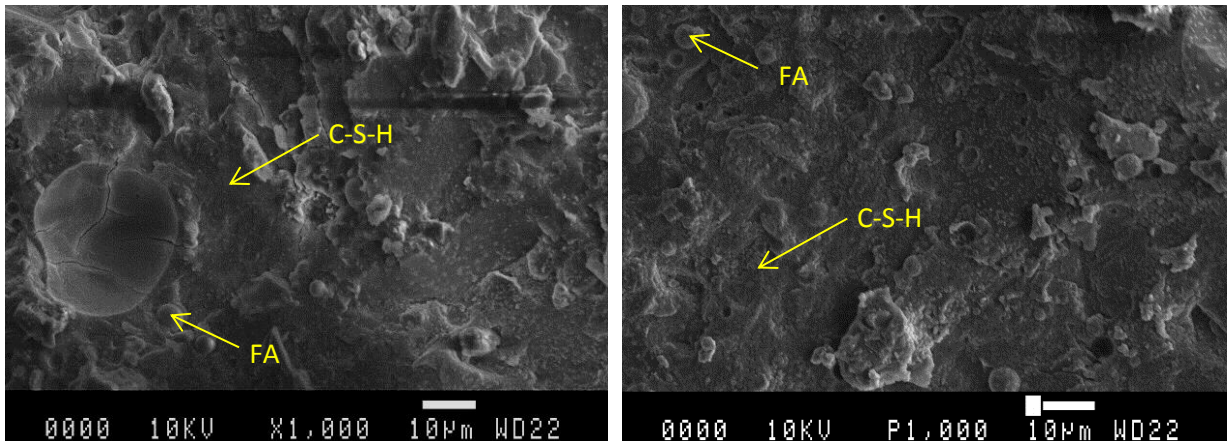
Figure 6. Scanning electron micrographs of the AAFS mixes at 28 days (a) GFM10N0; (b) GFM0N5; (c) GFM5N5; (d) GFM10N10

In all blends, C-S-H gel is the main feature of the microstructure with some fly ash remaining unreacted. That unreacted particles were easily found suggests that fly ash is not, at least at early ages, interacting with the cementing phase on a chemical level which is not unusual even in AAF (geopolymer) mixtures [10–12]. Regarding the C-S-H gel, it may belong to a low-crystalline calcium silicate hydrate rich in Al, which includes Na into its structure [12].

369 To determine the elemental composition of the hydration products, EDX were performed on

370 at least 20 points selected on the gels and some of the slag grains in some samples cured for

371 28 days at a magnification of 2500 on a backscattered mode. Fig. 8a shows that the Al/Si ratio

372 is very high for either a pure chain-structured C-A-S-H phase (Al/Si<0.2 [55]) or considerable

373 degree of crosslinking [56] so it corresponds to the presence of additional Al-rich products

374 intermixed with Al-substituted C-S-H gel [19]. The good correlation of Mg/Si with Al/Si

375 indicates the presence of hydrotalcite-like phases (Fig. 8-b), while the presence of a positive

376 x-axis intercept reveals the level of incorporation of Al in the C-S-H (Table 4). The addition

377 of MgO slightly changed the gel composition where higher Ca/Si, Al/Si and Mg/Si ratios

378 were detected. From this observation, it may be deducted that the additional alkalis and MgO

379 lead to immediate increased pH and therefore increased the dissolution rates of the Ca, Si, Al

380 ions into the solution [57]. The Al-substitution decreased with the increase of MgO content

381 due to the increased Al content in hydrotalcite-like phase which was also observed by [29].

382 The range of Na/Si in the investigated samples was from 0.18 to 0.7 as shown in Fig. 8c. The

383 role of Na in the structure of the reaction products is to balance the negative framework

384 charge induced by the incorporation of Al [12,58].

385 According to the EDX analysis, chemical composition of the gel could indicate the formation

386 of hybrid C-(N)-A-S-H gel or the coexistence of N-A-S-H and C-A-S-H intermixed with

387 hydrotalcite gel and M-S-H gel [29,59].

388   Table 4. Calculated parameters from EDS results at 28 days
389

Sample	Ca/Si	Al/Si	Mg/Si	Na/Si	Mg/Al (calculated from Fig. 8b)	Al substitution
Slag	1.19	0.40	0.36	0.09	0.7	-
GFM0N10	0.83	0.43	0.30	0.53	1.94	0.28
GFM5N10	1.17	0.48	0.45	0.41	1.63	0.19
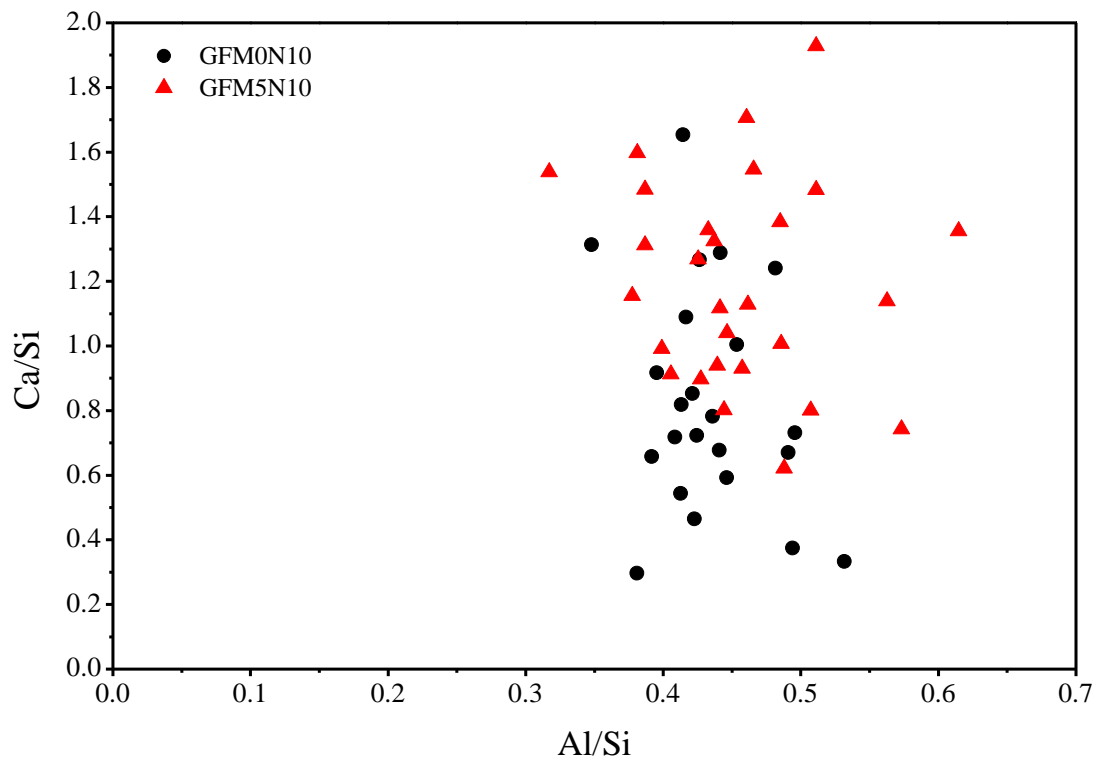
(a)
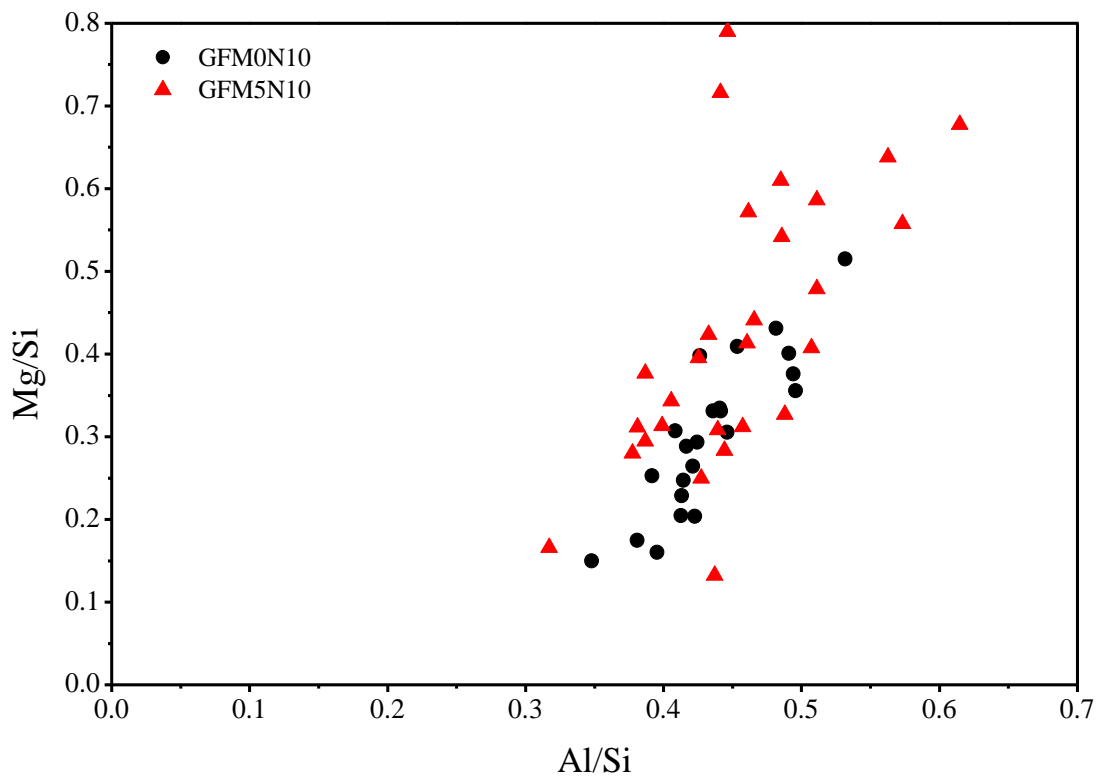
(b)
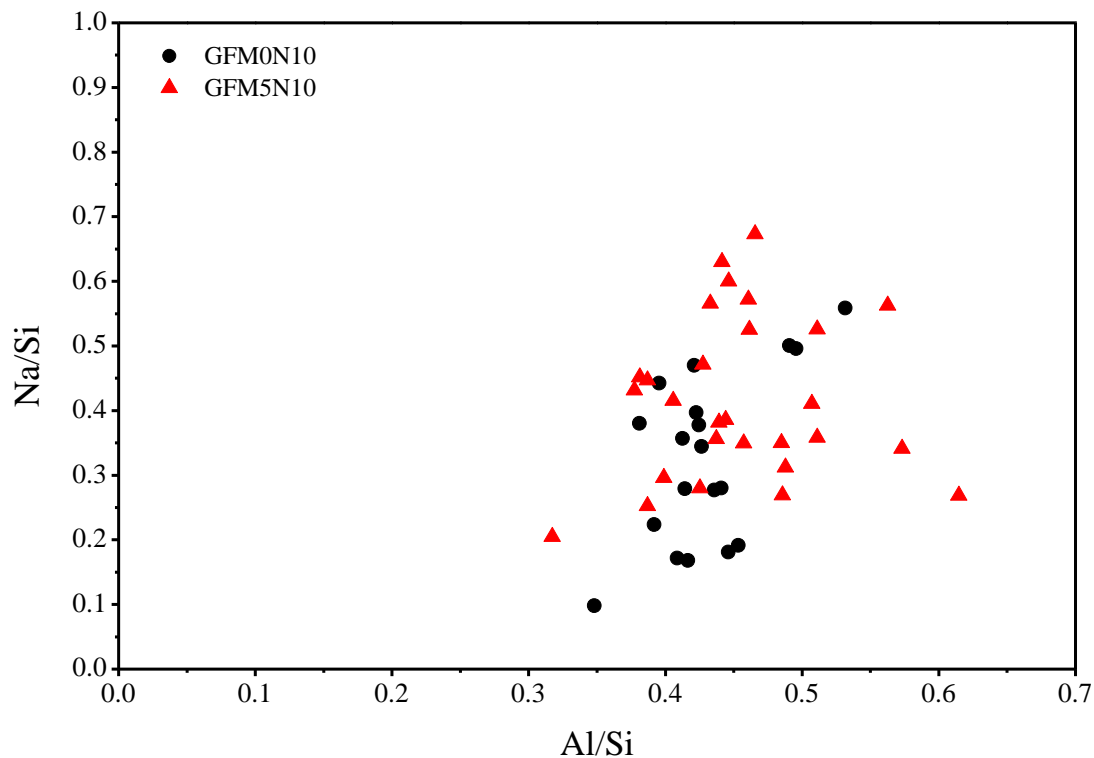
(c)

Figure 7. Atomic ratios for 10% Na_2CO_3 activated mixes with 0 and 5% MgO(A) Ca/Si vs Al/Si, (B) Mg/Si vs Al/Si, and (C) Al/Si vs Na/Si.

4. Conclusion

390

391   The strength of the AAFS mixes highly depends on the activator dosage and it was clear that

392   increasing the Na_2CO_3 dosage increased the strength at all ages. The highest strength obtained

393   was attributed to the paste mix consisting of slag:fly ash in 3:1 ratio and with 10% of both

394   Na_2CO_3 and MgO, which reached ~80 MPa at 90 days. It was found that incorporating MgO

395   to the blends had a notable influence on the reaction rate, and the microstructure of the mixes

396   and slight influence on the strength. These effects could be beneficial in accelerating the

397   setting time of these blends and the reduction of the shrinkage as will be reported in future

398   studies. The main hydration product was C-(N)-A-S-H gel as the binding phase in these

399   mixes. Furthermore, other hydration products such as hydrotalcite-like phases, calcite, and

400   gaylussite were formed.

5

References

[1]   U.S. Geological Survey, Mineral Commodity Summaries: Cement, 2013.

[2]   M. Schneider, M. Romer, M. Tschudin, H. Bolio, Sustainable Cement Production—Present and Future, Cem. Concr. Res. 41 (2011) 642–650.

[3]   D. Higgins, L. Sear, D. King, B. Price, R. Barnes, C. Clear, Cementitious Materials: The Effect of GGBS, Fly Ash, Silica Fume and Limestone Fines on the Properties of Concrete, Surrey, 2011.

[4]   B. Suhendro, Toward Green Concrete for Better Sustainable Environment, Procedia Eng. 95 (2014) 305–320.

[5]   M. Liska, A. Al-Tabbaa, Ultra-Green Construction: Reactive Magnesia Masonry Products, Proc. ICE - Waste Resour. Manag. 162 (2009) 185–196.

[6]   F. Pacheco-Torgal, J. Castro-Gomes, S. Jalali, Alkali-Activated Binders: A Review. Part 2. About Materials and Binders Manufacture, Constr. Build. Mater. 22 (2008) 1315–1322.

[7]   F. Pacheco-Torgal, J. Castro-Gomes, S. Jalali, Alkali-Activated Binders: A Review Part 1. Historical Background, Terminology, Reaction Mechanisms and Hydration Products, Constr. Build. Mater. 22 (2008) 1305–1314.

[8]   A.M. Rashad, A Comprehensive Overview about the Influence of Different Admixtures and Additives on the Properties of Alkali-Activated Fly Ash, Mater. Des. 53 (2014) 1005–1025.

[9]   A.A. Adam, Strength and Durability Properties of Alkali Activated Slag and Fly Ash-Based Geopolymer Concrete, PhD thesis, RMIT University, 2009.

[10]   J.I. Escalante García, K. Campos-Venegas, A. Gorokhovsky, A. Fernández, Cementitious Composites of Pulverised Fuel Ash and Blast Furnace Slag Activated by Sodium Silicate: Effect of Na_2O Concentration and Modulus, Adv. Appl. Ceram. 105 (2006) 201–208.

[11]   F. Puertas, A. Fernandez-Jimenez, Mineralogical and Microstructural Characterisation of Alkali-Activated Fly Ash/slag Pastes, Cem. Concr. Compos. 25 (2003) 287–292.

432 [12] F. Puertas, S. Martinez-Ramirez, T. Vazquez, S. Alonso, Alkali-Activated Fly Ash
433 /Slag Cement Strength Behaviour and Hydration Products, Cem. Concr. Res. 30 (2000)
434 1625–1632.

435 [13] M. Chi, R. Huang, Binding Mechanism and Properties of Alkali-Activated Fly
436 Ash/Slag Mortars, Constr. Build. Mater. 40 (2013) 291–298.

437 [14] J.S.J. Deventer, J.L. Provis, P. Duxson, D.G. Brice, Chemical Research and Climate
438 Change as Drivers in the Commercial Adoption of Alkali Activated Materials, Waste
439 and Biomass Valorization. 1 (2010) 145–155.

440 [15] H. Xu, J.L. Provis, J.S.J. Van Deventer, P. V Krivenko, Characterization of Aged Slag
441 Concretes, ACI Mater. J. 102 (2008) 131–139.

442 [16] S. Wang, K.L. Scrivener, P.L. Pratt, Factors Affecting the Strength of Alkali-Activated
443 Slag, Cem. Concr. Res. 24 (1994) 1033–1043.

444 [17] A. Fernández-Jiménez, Alkali-Activated Slag Mortars Mechanical Strength Behaviour,
445 Cem. Concr. Res. 29 (1999) 1313–1321.

446 [18] Y. Li, Y. Sun, Preliminary Study on Combined-Alkali–slag Paste Materials, Cem.
447 Concr. Res. 30 (2000) 963–966.

448 [19] S. Bernal, J.L. Provis, R.J. Myers, R. San Nicolas, J.S.J. van Deventer, Role of
449 Carbonates in the Chemical Evolution of Sodium Carbonate-Activated Slag Binders,
450 Mater. Struct. (2014) 1–13.

451 [20] M.A. Shand, The Chemistry and Technology of Magnesia, JOHN WILEY & SONS,
452 2006.

453 [21] Z. Lou, Q. Ye, H. Chen, Y. Wang, J. Shen, Hydration of MgO in Clinker and Its
454 Expansion Property, J. Chin. Ceram. Soc. 26 (1998) 430–436.

455 [22] X. Li, Mechanical Properties and Durability Performance of Reactive Magnesia
456 Cement Concrete, PhD thesis, University of Cambridge, 2012.

457 [23] Y. Yi, M. Liska, A. Al-Tabbaa, Properties and Microstructure of GGBS–magnesia
458 Pastes, Adv. Cem. Res. 26 (2014) 114–122.

459 [24] F. Jin, K. Gu, A. Abdollahzadeh, A. Al-Tabbaa, Effects of Different Reactive MgOs on
460 the Hydration of MgO-Activated GGBS Paste, J. Mater. Civ. Eng. (2013) 1–9.

461 [25] F. Jin, A. Al-Tabbaa, Characterisation of Different Commercial Reactive Magnesia,
462 Adv. Cem. Res. 26 (2014) 101–113.

463 [26] M. Ben Haha, B. Lothenbach, G. Le Saout, F. Winnefeld, Influence of Slag Chemistry
464 on the Hydration of Alkali-Activated Blast-Furnace Slag — Part I: Effect of MgO,
465 Cem. Concr. Res. 41 (2011) 955–963.

466 [27] W. Shen, Y. Wang, T. Zhang, M. Zhou, J. Li, X. Cui, Magnesia Modification of
467   Alkali-Activated Slag Fly Ash Cement, J. Wuhan Univ. Technol. Sci. Ed. 26 (2011)
468   121–125.

469 [28] T. Kwok, Sustainable Concrete Using Slag and Limestone, Fourth year project
470   report,Cambridge University Engineering Department, 2013.

471 [29] F. Jin, K. Gu, A. Al-Tabbaa, Strength and Drying Shrinkage of Reactive MgO
472   Modified Alkali-Activated Slag Paste, Constr. Build. Mater. 51 (2014) 395–404.

473 [30] F. Jin, A. Al-Tabbaa, Strength and Drying Shrinkage of Reactive MgO and Sodium
474   Carbonate Activated Slag Paste, Constr. Build. Mater. 2015 (accepted Publ. (2015).

475 [31] A. Abdalqader, A. Al-Tabbaa, Hydration and Mechanical Properties of Reactive
476   Magnesia and Sodium Carbonate-Activated Fly Ash/Slag Paste Blends, in: RILEM
477   PRO092 Proceeding Second Int. Conf. Adv. Chem. Mater. (CAM'2014-China), June
478   1-3, 2014, Chang. China, RILEM Publications S.A.R.L., Changsha, China, 2014: pp.
479   269–280.

480 [32] A.R. Sakulich, E. Anderson, C. Schauer, M.W. Barsoum, Mechanical and
481   Microstructural Characterization of an Alkali-Activated Slag/limestone Fine Aggregate
482   Concrete, Constr. Build. Mater. 23 (2009) 2951–2957.

483 [33] F. Jin, K. Gu, A. Al-Tabbaa, Strength and Hydration Properties of Reactive MgO-
484   Activated Ground Granulated Blastfurnace Slag Paste, Cem. Concr. Compos. 57
485   (2015) 8–16.

486 [34] Y. Yi, M. Liska, A. Al-Tabbaa, Initial Investigation into the Use of GGBS-MgO in Soil
487   Stabilisation, in: 4th Int. Conf. Grouting Deep Mix. 2012, American Society of Civil
488   Engineers, Reston, VA, 2012: pp. 444–453.

489 [35] L.J. Vandeperre, M. Liska, A. Al-Tabbaa, Mixtures of Pulverized Fuel Ash, Portland
490   Cement and Magnesium Oxide: Strength Evolution and Hydration Products, in: Sixth
491   Int. Conf. Sci. Eng. Recycl. Environ. Prot., Belgrade, 2006: pp. 539–550.

492 [36] L.J. Vandeperre, M. Liska, A. Al-Tabbaa, Hydration and Mechanical Properties of
493   Magnesia, Pulverized Fuel Ash, and Portland Cement Blends, J. Mater. Civ. Eng. 20
494   (2008) 375–383.

495 [37] A. Sakulich, Characterization of Environmentally-Friendly Alkali Activated Slag
496   Cements and Ancient Building Materials, PhD thesis, Drexel University, 2009.

497 [38] Y. Li, Y. Sun, Preliminary Study on Combined-Alkali-Slag Paste Materials, Cem.
498   Concr. Res. 30 (2000) 963–966.

499 [39] S. a. Bernal, R. San Nicolas, R.J. Myers, R. Mejía de Gutiérrez, F. Puertas, J.S.J. van
500   Deventer, et al., MgO Content of Slag Controls Phase Evolution and Structural

501 Changes Induced by Accelerated Carbonation in Alkali-Activated Binders, Cem.
502 Concr. Res. 57 (2014) 33–43.

503 [40] C. Shi, D. Roy, P. Krivenko, Alkali-Activated Cements and Concretes, Taylor &
504 Francis, Oxon, 2006.

505 [41] F. Mees, E. Reyes, E. Keppens, Stable Isotope Chemistry of Gaylussite and Nahcolite
506 from the Deposits of the Crater Lake at Malha, Northern Sudan, Chem. Geol. 146
507 (1998) 87–98.

508 [42] S. Bernal, J.L. Provis, D.G. Brice, A. Kilcullen, P. Duxson, J.S.J. van Deventer,
509 Accelerated Carbonation Testing of Alkali-Activated Binders Significantly
510 Underestimates Service Life: The Role of Pore Solution Chemistry, Cem. Concr. Res.
511 42 (2012) 1317–1326.

512 [43] J.L. Provis, J.S.J. van Deventer, eds., Alkali Activated Materials, Springer Netherlands,
513 Dordrecht, 2014.

514 [44] Y. Yi, M. Liska, A. Al-Tabbaa, Properties and Microstructure of GGBS-MgO Pastes,
515 Adv. Cem. Res. (2013).

516 [45] F. Jin, A. Al-Tabbaa, Thermogravimetric Study on the Hydration of Reactive Magnesia
517 and Silica Mixture at Room Temperature, Thermochim. Acta. 566 (2013) 162–168.

518 [46] P.C. Hewlett, ed., Lea's Chemistry of Cement and Concrete, fourth edi, Elsevier
519 Science & Technology Books, Oxford, 2004.

520 [47] I. Ismail, S. a. Bernal, J.L. Provis, S. Hamdan, J.S.J. Deventer, Microstructural
521 Changes in Alkali Activated Fly Ash/slag Geopolymers with Sulfate Exposure, Mater.
522 Struct. 46 (2013) 361–373.

523 [48] M. Földvári, Handbook of the Thermogravimetric System of Minerals and Its Use in
524 Geological Practice, 213th ed., Geological Institute of Hungary, Budapest, 2011.

525 [49] I. Ismail, S. Bernal, J. Provis, R. San Nicolas, D.G. Brice, A.R. Kilcullen, et al.,
526 Influence of Fly Ash on the Water and Chloride Permeability of Alkali-Activated Slag
527 Mortars and Concretes, Constr. Build. Mater. 48 (2013) 1187–1201.

528 [50] M. Ben Haha, G. Le Saout, F. Winnefeld, B. Lothenbach, Influence of Activator Type
529 on Hydration Kinetics, Hydrate Assemblage and Microstructural Development of
530 Alkali Activated Blast-Furnace Slags, Cem. Concr. Res. 41 (2011) 301–310.

531 [51] I. Garcia-Lodeiro, a. Palomo, a. Fernández-Jiménez, D.E. Macphee, Compatibility
532 Studies between N-A-S-H and C-A-S-H Gels. Study in the Ternary Diagram Na2O–
533 CaO–Al2O3–SiO2–H2O, Cem. Concr. Res. 41 (2011) 923–931.

534 [52] C.A. Rees, J.L. Provis, G.C. Lukey, J.S.J. Van Deventer, Attenuated Total Reflectance
535   Fourier Transform Infrared Analysis of Fly Ash Geopolymer Gel Aging, Langmuir. 23
536   (2007) 8170–8179.

537 [53] A. Hajimohammadi, J.L. Provis, J.S.J. Van Deventer, One-Part Geopolymer Mixes
538   from Geothermal Silica and Sodium Aluminate, Ind. Eng. Chem. Res. 47 (2008) 9396–
539   9405.

540 [54] W. Mozgawa, J. Deja, Spectroscopic Studies of Alkaline Activated Slag Geopolymers,
541   J. Mol. Struct. 924-926 (2009) 434–441.

542 [55] W. Hunnicutt, Characterization of Calcium-Silicate-Hydrate and Calcium-Alumino-
543   Silicate-Hydrate, Master thesis, University of Illinois at Urbana-Champaign, 2013.

544 [56] R.J. Myers, S. Bernal, R. San Nicolas, J.L. Provis, Generalized Structural Description
545   of Calcium-Sodium Aluminosilicate Hydrate Gels: The Cross-Linked Substituted
546   Tobermorite Model., Langmuir. 29 (2013) 5294–306.

547 [57] E. Deir, B.S. Gebregziabiher, S. Peethamparan, Influence of Starting Material on the
548   Early Age Hydration Kinetics, Microstructure and Composition of Binding Gel in
549   Alkali Activated Binder Systems, Cem. Concr. Compos. 48 (2014) 108–117.

550 [58] P. Duxson, A. Fernández-Jiménez, J.L. Provis, G.C. Lukey, A. Palomo, J.S.J.
551   Deventer, Geopolymer Technology: The Current State of the Art, J. Mater. Sci. 42
552   (2006) 2917–2933.

553 [59] N. Marjanović, M. Komljenović, Z. Baščarević, V. Nikolić, R. Petrović, Physical–
554   mechanical and Microstructural Properties of Alkali-Activated Fly Ash–blast Furnace
555   Slag Blends, Ceram. Int. 41 (2015) 1421–1435.